Level density and thermodynamics in the hot rotating ^{96}Tc nucleus

Balaram Dey,[1,*] Deepak Pandit,[2] Srijit Bhattacharya,[3] N. Quang Hung,[4,†] N. Dinh Dang,[5,6] L. Tan Phuc,[4,7]
Debasish Mondal,[2,8] S. Mukhopadhyay,[2,8] Surajit Pal,[2] A. De,[9] and S. R. Banerjee[2]

[1]*Department of Nuclear and Atomic Physics, Tata Institute of Fundamental Research, Mumbai-400005, India*

[2]*Variable Energy Cyclotron Centre, 1/AF-Bidhannagar, Kolkata 700064, India*

[3]*Department of Physics, Barasat Govt. College, Barasat, N 24 Pgs, Kolkata 700124, India*

[4]*Institute of Fundamental and Applied Sciences, Duy Tan University, 3 Quang Trung, Danang City-551300, Vietnam*

[5]*Quantum Hadron Physics Laboratory, RIKEN Nishina Center for Accelerator-Based Science, RIKEN, 2-1 Hirosawa, Wako City, Saitama 351-0198, Japan*

[6]*Institute of Nuclear Science and Technique, Hanoi-122100, Vietnam*

[7]*Faculty of Physics and Engineering Physics, Vietnam National University Ho Cho Minh City - University of Science, Ho Chi Minh City-748355, Vietnam*

[8]*Homi Bhabha National Institute, Training School Complex, Anushaktinagar, Mumbai-400094, India*

[9]*Department of Physics, Raniganj Girls' College, Raniganj 713358, India*

Evaporated neutron energy spectra have been measured in coincidence with low-energy discrete γ rays in the reaction ^{4}He + ^{93}Nb at $E(^4\text{He}) = 28$ MeV. The low-energy light-ion beam provides the scope of extracting the experimental nuclear level density (NLD) in the compound nuclear reaction. Angular-momentum gated NLDs have been extracted in the excitation energy range of $E^* \sim 5$–15 MeV from the measured neutron energy spectra. The extracted NLDs have been compared with different theoretical calculations such as the exact pairing plus independent particle model at finite temperature (EP+IPM), Hartree-Fock plus BCS (HFBCS), and Hartree-Fock-Bogoliubov plus combinatorial method (HFBC). Interestingly, the experimental NLDs are in good agreement with the results of the EP+IPM, whereas the HFBCS and HFBC fail to describe these data. Consequently, the thermodynamic properties of ^{96}Tc at finite angular momentum have been extracted using the EP+IPM NLDs. Through the analysis of the calculated thermodynamic quantities, it is shown that no pronounced bump is seen in the heat capacity of ^{96}Tc, in opposition with the earlier results of ^{96}Mo, which showed a prominent bump at $T \sim 0.7$–1 MeV. This difference is understandable since pairing in the even-even system (^{96}Mo) is always stronger than that in the odd-odd one (^{96}Tc).

I. INTRODUCTION

One of the basic aims in diverse fields of science (physics, chemistry, and biology) is understanding the small system, which manifests many striking properties due to its tiny dimension. Some popular examples of such systems are atomic nuclei, nanoparticles, magnetic domain in ferromagnets, quantum dots, biological molecular machines, and solidlike clusters, which are important in the relaxation of glassy systems, etc. [1]. The study of thermodynamic properties of these systems, in spite of being an arduous task, is highly imperative as those properties describe how such systems respond to the changes in their environment [2].

The atomic nucleus is a well-known example of a small system, which shows the prototypical behavior of a complex miniature arrangement that goes beyond the simple sum of individual nucleon properties. Nuclear thermodynamics was essentially initiated by Bethe in 1936 [3], which explains the nuclear bulk properties instead of the individual nucleon ones and demonstrates the energy exchange process of a macroscopic system [4]. The knowledge of nuclear thermodynamics

also enables us to understand the presence of pairing phase transition in the nucleus, whose effect was included in the nuclear theory after the Bardeen-Cooper-Schrieffer (BCS) theory [5]. As a result, the study of nuclear thermodynamics has gained much enthusiasm in the recent past [6–9].

Measuring the nuclear level density (NLD) is the starting point to obtain the thermodynamic quantities (TQs) of atomic nuclei. The introduction of the collective enhancement into the description of NLD has removed many contradictions of the previous analyses of experimental data, as has been reviewed in detail in Ref. [6]. In the past, nuclear researchers lacked proper experimental methods to measure the TQ until recently, when nuclear experimentalists proposed a unique technique to simultaneously extract the NLD and radiative γ-ray strength function [10]. This achievement has opened up a new horizon in this field. They have extracted the level density for $^{93-98}$Mo and obtained the S-shape canonical heat capacity as an indication of pairing phase transition at a critical temperature of $T_c = 0.7$–1.0 MeV [11,12]. In the recent past, Schiller *et al.* [7] and Melby *et al.* [8] observed steplike structures in the level densities around excitation energy $E^* \sim 1$–7 MeV, most probably because of the breaking of nucleon Cooper pairs, which leads to a gradual decrease of pairing correlations. However, they have extracted the level density below the particle threshold energy at very low angular momentum J

---

*Present address: Saha Insititue of Nuclear Physics, 1/AF-Bidhannagar, Kolkata 700064, India; dey.balaram@gmail.com

†nqhungdtu@gmail.com

(a few $\hbar$) and extrapolated it to the higher energy using the functional form of the Fermi gas (FG) model [3] to estimate the TQ. However, the knowledge of NLD functional form is not yet satisfactory due to the lack of experimental data at high E^* and J. Therefore, it would be better if one could measure the NLD below and above the particle threshold, and compare the measured data with a consistent theoretical calculation to investigate thermodynamic properties of atomic nuclei. On the other hand, the inverse level density parameter, which is an important ingredient in the functional form of the FG model [3], should be measured experimentally as it varies strongly with T and J [13–16]. In addition, all the reported information on nuclear thermodynamics is at a very low J (a few $\hbar$). Till now, there is no information of nuclear thermodynamics at a higher J, that is, a question still remains on how angular momentum affects the thermodynamic behavior of atomic nucleus.

Precise measurement of NLD is a very difficult task due to the lack of proper experimental technique. The nuclear levels can be divided into two energy regions, namely the low-energy discrete region (below 3–5 MeV) and the high-energy continuum one (>5 MeV). In the low-energy region, the NLD is directly measured by counting the discrete levels, whereas above the region of discrete levels, it is measured by using some model-based functions (constant temperature formula, Fermi Gas model, etc.) with some parameters (level density parameter, spin cutoff factor, etc.). The parameters in the model-based function are either taken from the systematics or experimentally measured. There are several approaches to experimentally estimate the NLD above the discrete region. One of them is the Oslo method, which extracts the NLD from the particle-γ coincidence matrices by using inelastic scattering and/or transfer reactions [10]. Another one is by measuring the particle evaporation spectra from compound nuclear reactions [17,18]. The Oslo method is limited to a region of low excitation energy (up to the particle threshold) and low J (a few $\hbar$), whereas it is possible to extract the NLD beyond or below the particle threshold at higher J by using the particle evaporation technique. The major problem with the particle evaporation technique is the possible contributions from the multistep and direct reactions. However, the use of a low-energy light-ion beam (α) could provide the scope for extracting the NLD from a particular channel and the contributions from direct reaction can be ruled out by measuring the particle spectra at backward angle. The consistency of these two experimental techniques has been checked in Ref. [18], where it has been shown that particle spectra are most suitable for NLD studies.

In the present work, the angular momentum gated NLDs in the excitation energy range of $E^* \sim 5$–15 MeV are extracted by using the evaporated neutron energy spectra in the $^4\text{He} + ^{93}\text{Nb}$ reaction. The advantage of using the light-ion beam is that, at lower excitation energy, the compound nucleus mainly decays via the $1n$ channel and thus produces the residual nucleus ^{96}Tc. Angular momentum information is extracted by measuring the low-energy discrete γ rays. The inverse level density parameter (k), an important ingredient in the calculation of NLD, is also measured directly in our experiment. The extracted NLD is then compared with the results of different microscopic calculations and the best matched

NLD has been used to investigate the thermodynamics of ^{96}Tc at different T and J. In addition, the spin cutoff factor as a function of excitation energy has also been extracted from the ratio of NLDs at different angular momenta.

II. EXPERIMENTAL DETAILS AND ANALYSIS

The experiments were carried out at the Variable Energy Cyclotron Center, Kolkata using a light-ion α beam from the K-130 cyclotron. A self-supporting 1 mg/cm^2 thick ^{93}Nb target (99.9% enriched) was bombarded by α beam at 28 MeV populating ^{97}Tc nucleus at the initial excitation energy of 29.3 MeV. A liquid organic scintillator-based (BC501A) neutron detector [19], placed at a distance of 150 cm from the target position, was used to detect the evaporated neutrons in coincidence with the low-energy discrete γ rays. The neutron detector was placed at a backward angle of 125° with respect to the beam direction in order to remove the contributions from the direct reaction. A 50-element low-energy γ-multiplicity filter [20] was used to detect those low-energy discrete γ rays in order to make an angular momentum gated measurements. The multiplicity filter (consisting of 50 BaF$_2$ detectors, each having dimension of $3.5 \times 3.5 \times 5$ cm^3) was split into two blocks of 25 detectors each, in a staggered castle-type geometry to equalize the solid angle for each multiplicity detector element, and placed at a distance of 5 cm above and below the center
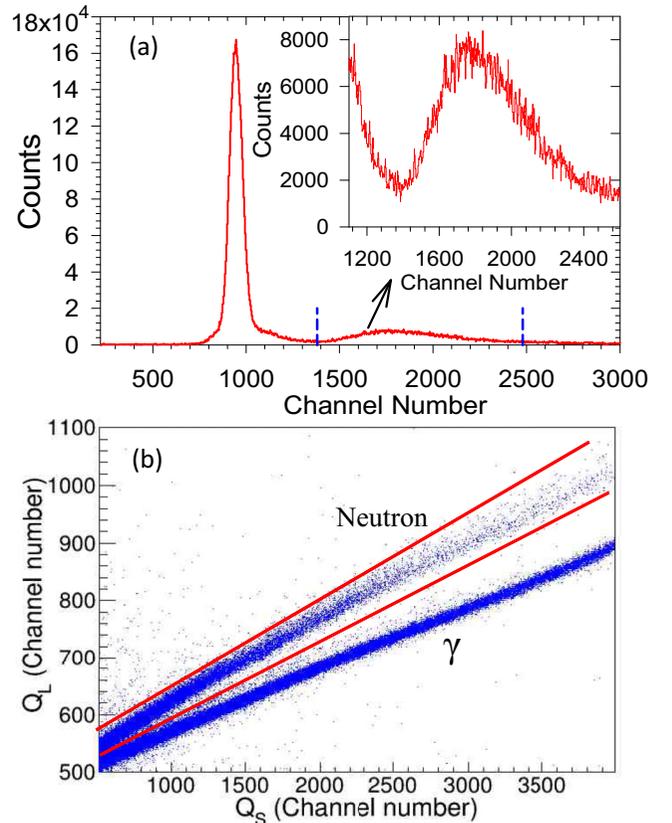

FIG. 1. (a) Time-of-flight and (b) pulse shape discrimination (bottom panel) spectra in the reaction of $^4\text{He} + ^{93}\text{Nb}$ at $E_{\text{lab}}(^4\text{He}) =$ 28 MeV. Q_L and Q_S are the charge integrated over the long ($2\,\mu s$) and short integration (50 ns) gate widths, respectively.

of scattering chamber. The efficiency of the multiplicity setup was 56% as calculated using the GEANT4 simulation [21].

The evaporated neutrons were measured by the time-of-flight (TOF) technique. The START trigger was generated from the γ-multiplicity filter when at least one detector, each from the top and bottom blocks, fired in coincidence, above an energy threshold of 250 keV. The STOP trigger was generated when the signal in the neutron detector crossed a threshold of 250 keV. The neutron-γ discrimination was achieved by both the pulse shape discrimination (PSD) and TOF techniques. The typical TOF and PSD spectra obtained from the present experiment are shown in Fig. 1. The event was recorded when both top and bottom multiplicity detectors fired in coincidence with the signal (with the threshold >250 keV) from the neutron detector. The beam dump was heavily shielded with lead bricks and borated paraffin to keep the background of the detectors at a minimum level. A CAMAC-based electronics and VME-based data acquisition system were used to simultaneously record the energy and time information of the detectors.

The neutron TOF spectrum was converted to the energy spectrum using the prompt γ peak as a time reference. The efficiency correction for the neutron detector was performed using GEANT4 simulation code [21]. The multiplicity folds (the number of detectors fired) were obtained by measuring the low-energy discrete γ rays. The experimental fold distribution of the multiplicity filter was converted to the angular momentum distribution using the GEANT4 simulation with the approach discussed in Ref. [20]. The uncertainty in the extracted angular momentum was $\pm 4\hbar$. The fold and angular-momentum distributions are shown in Fig 2. The fold-gated neutron energy spectra are shown in Fig. 3. The error bars shown in Fig. 3 are due to counting statistics only.

III. DESCRIPTION OF NUCLEAR LEVEL DENSITY BY USING STATISTICAL MODEL

The fold-gated neutron energy spectra were fitted to the statistical model CASCADE [22] calculations with the NLD prescription (FG model) [3] given by

$$\rho(E^*, J) = \frac{2J+1}{12\theta^{3/2}} \sqrt{a} \frac{\exp(2\sqrt{aU})}{U^2}, \qquad (1)$$

where, $\theta = \frac{2I_{eff}}{\hbar^2}$, I_{eff} is the effective rigid-body moment of inertia, a is the level density parameter. The available energy is $U = E^* - \frac{J(J+1)}{\theta} - S_n - \Delta P$, where S_n and ΔP are the neutron separation energy and pairing energy, respectively. In the CASCADE calculation, the Ignatyuk's prescription of level density parameter a was adopted [23], which takes into account the nuclear shell effects at low excitation energy and connects smoothly to the liquid drop value at high excitation. The Ignatyuk's prescription is given by

$$a = \tilde{a}\left\{ 1 - \frac{\Delta S}{U}[1 - \exp(-\gamma U)] \right\}, \qquad (2)$$

where $\gamma = \frac{0.4A^{4/3}}{\tilde{a}}$, $\tilde{a}$ ($=A/k$) is the asymptotic Fermi gas value of the liquid-drop NLD parameter at the excitation energy where shell effects melt, leaving a smooth dependence on nu-
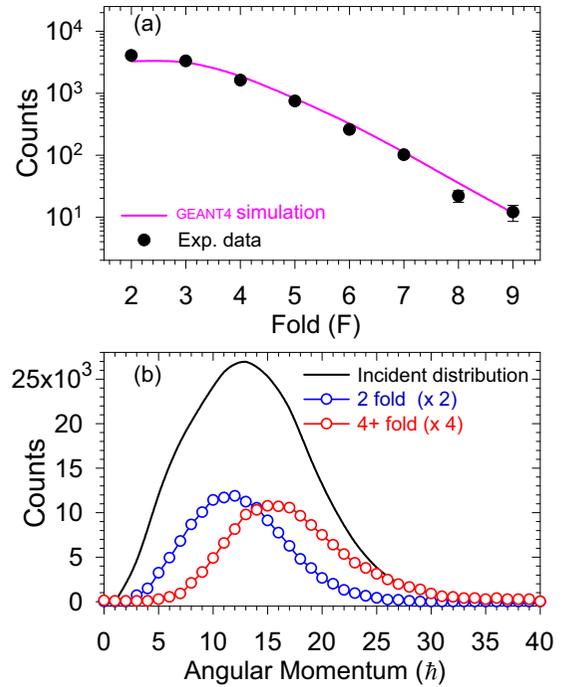

FIG. 2. (a) Experimental fold distribution along with the GEANT4 simulation. (b) Angular momentum distribution for different folds (F) for the ^{4}He + ^{93}Nb reaction at 28 MeV incident energy.

clear mass A, whereas ΔS is the shell correction obtained from the difference of the experimental and the liquid-drop model masses and γ is the rate at which the shell effect damps with increasing the excitation energy. The transmission coefficients for the statistical model calculation are obtained from the optical model. The potential parameters for neutron, proton, and α are taken from Refs. [24–26], respectively. The moment of inertia of the CN is taken as $I_{eff} = I_0(1 + \delta_1 J^2 + \delta_2 J^4)$, where $I_0 (= \frac{2}{5}MA^{5/3}r_0^2)$ is the moment of inertia of a spherical nucleus, δ_1 and δ_2 are the deformability parameters, and r_0 is the radius parameter. The values of δ_1 and δ_2 used in the CASCADE code are 2×10^{-5} and 2×10^{-8}, respectively. The role of the deformability parameters δ_1 and δ_2 is found to be inconsequen-
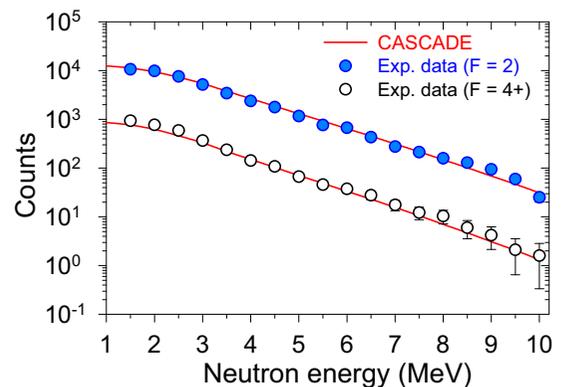

FIG. 3. Evaporated neutron energy spectra (filled circles) along with results of the statistical model calculations (continuous line) for different folds (F).
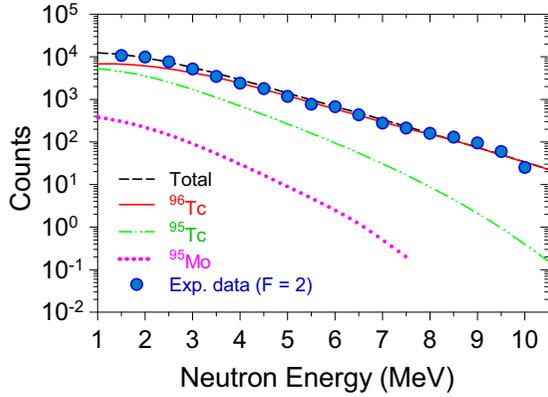
FIG. 4. Neutron contribution (CASCADE) from different channels along with experimental data for fold $F = 2$.

tial and the shape of neutron energy spectra depends mostly on the level density parameter. The neutron energy spectra along with the best-fitted CASCADE calculations are shown in Fig. 3.

The measurable quantities in Eq. (1) are the angular momentum (J) and inverse level density parameter ($k = A/\widetilde{a}$). The angular-momentum distribution was extracted from the experimental fold distributions and was used as inputs for different folds in the CASCADE code. The inverse level density parameter was estimated from the experimental neutron spectra after the best fitting with statistical model calculation using a χ^2-minimization technique within the energy range of 3–9 MeV (see, e.g., Fig. 3). Thereafter, the measured neutron energy spectra, best-fitted spectra, k and J are used in the FG model (1) to extract the experimental NLD using the equation following the approach presented in Refs. [17,27,28], namely

$$\rho_{\text{exp}}(E_X) = \rho_{\text{fit}}(E_X)\frac{(d\sigma/dE)_{\text{exp}}}{(d\sigma/dE)_{\text{fit}}}. \quad (3)$$

Here, $(d\sigma/dE)_{\text{exp}}$ and $(d\sigma/dE)_{\text{fit}}$ are the experimental neutron evaporation and best-fitted theoretical spectra, respectively. The excitation energy is $E_X = U - E_n^{\text{CM}}$, where E_n^{CM} is the neutron energy in the center-of-mass frame. The quantity $\rho_{\text{fit}}(E_X)$ is the best-fitted level density taken from CASCADE calculation as has been discussed above.

To identify the predominant contributor, the neutron evaporation spectra from different nuclei in the decay chain of the CN were extracted from the CASCADE code and are displayed in Fig. 4 along with the total neutron energy spectra. It can be clearly seen that the contribution in the neutron energy of 3–10 MeV is mainly dominated by the $1n$ channel, producing the residual nucleus ^{96}Tc. The contribution of 1n channel with respect to the $2n$ channel in this energy range is ∼90%. Hence, in this case, the extraction of the experimental level density parameter using χ^2 minimization in the energy range of 3–9 MeV enables one to select the contribution mostly from the ^{96}Tc nucleus.

IV. MICROSCOPIC DESCRIPTION OF NUCLEAR LEVEL DENSITY

The experimental data are compared with results of the microscopic calculation based on the exact solutions

of the pairing Hamiltonian for a given number of single-particle levels around the Fermi surface in combination with the independent-particle model for the remaining portion of the single-particle spectrum (EP+IPM) [29]. The details of this microscopic model are given below.

The model considers the pairing Hamiltonian describing a system of neutrons (ν) and protons (π) moving in the corresponding mean-field potentials and interacting via monopole pairing forces with constant parameters G_τ ($\tau = \nu, \pi$). The Hamiltonian is taken in its usual form as

$$H = \sum_k \epsilon_k(a_k^\dagger a_k + a_{-k}^\dagger a_{-k}) - \sum_\tau G_\tau \sum_{k,k'}^\tau a_k^\dagger a_{-k}^\dagger a_{-k'} a_{k'}, \quad (4)$$

where $a_{\pm k}^\dagger$ and $a_{\pm k}$ denote the particle creation and annihilation operators, respectively, on the kth single-particle levels in the deformed basis. This Hamiltonian can be diagonalized to find all the exact eigenvalues $\mathcal{E}^S$ and single-particle occupation numbers f_k^S at different total seniorities S [30], which stand for the total numbers of unpaired particles. These exact solutions are then embedded into the CE to construct the exact partition function at $T \neq 0$ as [31]

$$Z_{\text{CE}}(\beta) = \sum_S d_S e^{-\beta\mathcal{E}^S}, \quad (5)$$

where $d_S = 2^S$ is the degeneracy and $\beta = 1/T$ is the inverse of temperature. Because the size of the matrix to be diagonalized in the pairing Hamiltonian (4) cannot be too large, this exact CE partition function is limited to the description of thermal properties only of the levels around the Fermi surface. To find the total partition function of the whole system, this exact CE partition function is combined with those obtained within the IPM by using Eq. (15) of Ref. [32], under the assumption that pairing is negligible for the levels far from the Fermi surface. The total partition function obtained in this way becomes

$$\ln Z' = \ln Z'_{\text{tr}} + \ln Z'_{\text{sp}} - \ln Z'_{\text{sp,tr}}, \quad (6)$$

where Z' is defined as the partition function with respect to the ground-state energy $\mathcal{E}_0$, namely $Z' \equiv Z e^{\beta\mathcal{E}_0}$ with $Z = Z_{\text{CE}}(\beta)$ in Eq. (5). In Eq. (6), Z'_{tr} is the CE partition function for the truncated single-particle spectrum, which consists of the levels around the Fermi surface; Z'_{sp} is the partition function obtained within the IPM for the entire single-particle spectrum from the bottom of the potential up to the closed shell with $N = 126$, whereas $Z'_{\text{sp,tr}}$ is the same partition function but for the truncated single-particle spectrum around the Fermi surface, which is already used for calculating Z'_{tr}. Based on the partition function (6), one can easily calculate all the nuclear TQ following the standard equations discussed in Ref. [3]. As a result, the density of states $\omega(E^*)$ at temperature $T = \beta_0^{-1}$ is calculated approximately by applying the method of steepest descent in evaluating the Laplace transformation of the partition function as [33]

$$\omega(E^*) = e^{S(E^*)}\left(-2\pi\frac{\partial\mathcal{E}}{\partial\beta_0}\right)^{-1/2}, \quad (7)$$

where

$$E^*(T) = \mathcal{E}(T) - \mathcal{E}(T = 0) \qquad (8)$$

is the excitation energy of the system. For spherical nuclei at high E^*, the NLD $\rho(E^*, M)$ at a given z projection of angular momentum J can be estimated from the density of states $\omega(E^*)$ by using the Gaussian approximation as [33,34]

$$\rho(E^*, M) \simeq \frac{\omega(E^*)}{\sigma\sqrt{2\pi}} \exp\left[-\frac{M}{2\sigma^2}\right]. \qquad (9)$$

The NLD $\rho(E, J)$ at a given total spin J can be then obtained as the difference between the level density with z projection $M = J$ and that with $M = J + 1$ as [33–35]

$$\rho(E, J) = \rho(E, M = J) - \rho(E, M = J + 1)$$
$$\simeq \frac{2J + 1}{2\sigma^3\sqrt{2\pi}} \omega(E) \exp\left[-\frac{J(J + 1)}{2\sigma^2}\right], \quad (10)$$

where σ is the spin cutoff parameter depending on the nuclear moment of inertia $\mathcal{I}$ as $\sigma_{\perp(\parallel)}^2 = \mathcal{I}_{\perp(\parallel)}T/\hbar^2$ with $\mathcal{I}_{\perp(\parallel)}$ being the moment of inertia perpendicular (parallel) to the symmetry axis of the nucleus. The perpendicular spin cutoff parameter is empirically given based on the limit of rigid body [36]

$$\sigma_\perp^2 \approx 0.015 A^{5/3} T. \qquad (11)$$

The parallel spin cutoff factor $\sigma_\parallel$ is obtained from $\sigma_\perp$ by using the empirical relation [37]

$$\sigma_\perp^2 = \sigma_\parallel^2 \frac{1 + \beta_2/3}{1 - 2\beta_2/3}, \qquad (12)$$

where β_2 is the quadrupole deformation parameter. For spherical and deformed nuclei, the collective and rotational degrees of freedom, which strongly enhance the level density but are not taken into account in the Hamiltonian (4), should be included in the NLD. As a result, instead of Eq. (10), one obtains the approximate formulas of the total NLD ρ_{vib} for (quasi)spherical nuclei and ρ_{rot} for well-deformed ones as [34]

$$\rho_{\mathrm{vib}}(E, J) \approx \frac{2J + 1}{2\sigma_\parallel^3\sqrt{2\pi}} \frac{\omega(E)}{(1 - e^{-\beta\Omega_\lambda})^{2\lambda+1}} \exp\left(-\frac{J(J + 1)}{2\sigma_{\parallel}^2}\right), \qquad (13)$$

$$\rho_{\mathrm{rot}}(E, J) \approx \frac{1}{2\sigma_\parallel\sqrt{2\pi}} \omega(E)$$
$$\times \sum_{K=-J}^{J} \exp\left[-\frac{K^2}{2\sigma_\parallel^2} - \frac{J(J + 1) - K^2}{2\sigma_\perp^2}\right], \qquad (14)$$

with Ω_λ in Eq. (13) being the phonon energy of the vibrational excitation corresponding to the phonon multipolarity λ, and the projection K of total angular momentum J on the symmetry axis in Eq. (14). The calculation of $\rho_{\mathrm{vib}}(E, J)$ includes the two most important multipole excitations, namely the quadrupole ($\lambda = 2$) and the octupole ($\lambda = 3$) ones, whose energies are taken from the experimental data of the first 2^+ and 3^- states. The collective enhancement has also been included in the original calculations of the NLD within the EP+IPM by using empirical formulas for the collective vibrational and rotational enhancement factors [29].

Given the NLD (13) or (14), one can construct the partition function of the nucleus at a given J and T, making use of the inverse Laplace transformation for the level density [38] as

$$Z(\beta, J) = \sum \rho(E, J)e^{-\beta E}\delta E, \qquad (15)$$

where $\rho(E, J)$ is obtained from Eq. (13) or (14). Knowing the partition function, one can compute all the TQ of a nucleus at different T and J by using the standard equations discussed in Ref. [3], except that the thermodynamic entropy $S(T)$ should be calculated based on the Clausius definition $dS = \beta d\overline{E}$ [31], namely

$$S = \int_0^T \frac{1}{\tau} C(T)d\tau, \qquad (16)$$

where $C(T) = \frac{\partial \overline{E}(T)}{\partial T}$ is the heat capacity. Consequently, the free energy $F(T)$ is calculated from $F = \overline{E} - TS$, where $\overline{E} = T^2 \frac{\partial}{\partial T}[\ln Z(T)]$. The reason for using Eq. (16) is due to the well-known unphysical divergence of the saddle-point approximation at very low E, from which the J-dependent partition functions (15) as well as the TQ are calculated [38]. This divergence sometimes leads to a negative value of the entropy at very low T if it is calculated by using the expression $S = (F - \overline{E})/T$.

The numerical calculations are performed for the nucleus ^{96}Tc, whose single-particle spectra are obtained within the axially deformed Woods-Saxon potential with the quadrupole deformation parameter β_2 equal to 0.16 [39]. The diagonalization of the pairing Hamiltonian (4) is carried out for 12 doubly degenerate single-particle levels, with six levels located above and the other six levels below the Fermi surface [29]. The blocking effect by the odd nucleon is properly taken into account. The pairing interaction parameters G_τ are chosen as $G_N = 0.47$ MeV and $G_Z = 0.42$ MeV for neutrons and protons, respectively, so that the neutron and proton exact pairing gaps at $T = 0$ reproduce their corresponding values obtained from the experimental odd-even mass differences [31]. The neutron and proton BCS gaps collapse at the critical temperatures T_c equal to 0.95 MeV and 0.84 MeV, respectively. Meanwhile the exact pairing gaps do not vanish, but monotonically decrease with increasing T at $T > 0.6$ MeV and remain finite in the range between 0.4–0.6 MeV even at $T = 4$ MeV, smoothing out the sharp phase transition from superfluid phase to the normal one in the BCS theory, as shown in Fig. 5. This feature of the exact pairing has been discussed thoroughly in the past (see, e.g., Refs. [29,31]). The slight increase of the exact gaps with T at $T \leqslant 0.6$ MeV is caused by the weakening of odd-particle blocking at low T as has been studied in Ref. [42].

The TQ at $J = 12$ and $16\hbar$ are calculated by using the partition function (15) with the NLD $\rho(E, J)$ obtained from Eq. (14) because the ^{96}Tc nucleus under consideration is asymmetrically deformed with positive value of $\beta_2 = 0.16$. These calculated $\rho(E, J)$ are then compared with the corresponding experimental data as well as those obtained within other approaches such as the Hartree-Fock BCS [43] and Hartree-Fock-Bogoliubov plus combinatorial methods (HFBC) for positive and negative parities [44].

It is worth noticing that the theoretical calculations of the NLD within the EP+IPM do not require the knowledge of the level density parameter a, which is a Fermi gas concept. It can
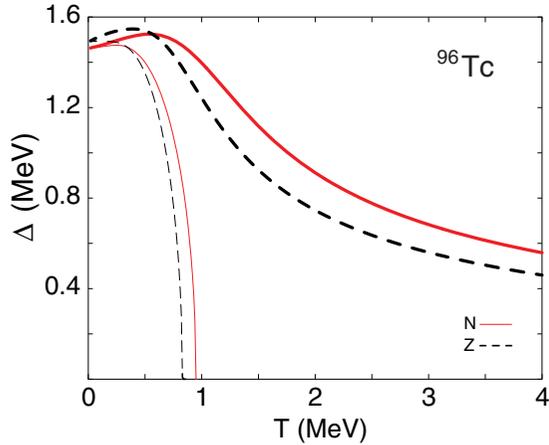
FIG. 5. Neutron and proton pairing gaps for ^{96}Tc as functions of temperature. The thick and thin lines denote the exact and BCS results, respectively.

be estimated from the theoretical excitation energy E^* (8) by using the Fermi gas formula $E^* = aT^2$. The spin cutoff factor $\sigma_\parallel^2$ can also be estimated microscopically in terms of the single-particle spin projection m_k and quasiparticle energies E_k as in Ref. [35]. This would allow us to study how the moment of inertia depends on the nuclear superfluidity and temperature as has been shown in Fig. 17 of Ref. [6], but by using the EP+IPM instead of the BCS pairing. However, this is beyond the scope of the present work, where the EP+IPM calculations are employed to support the experimental measurements of NLDs alone.

V. RESULTS AND DISCUSSIONS

A. Experimental and theoretical nuclear level densities

The experimental level density along with the results of different theoretical calculations for $J = 12$ and $16\,\hbar$ are shown in Fig. 7. The level density parameter and angular momentum were measured and used in the CASCADE code to calculate the level density. The uncertainty in the level density due to the statistical model parameter (such as different systematics of optical model parameter, radius parameter, diffuseness, etc.) has been checked and found to be ∼10%. The low-energy NLD data (∼1 MeV, represented by the open circles in Fig. 7) are obtained from the total NLD, which is calculated by counting the number of the experimental discrete levels taken from Ref. [45]. These low-energy data are multiplied by the spin distribution $f(J) = (2J + 1)\exp[-J(J + 1)/2\sigma^2]/[2\sigma^3\sqrt{2\pi}]$ with σ^2 being the spin cutoff factor taken from the systematics and weighted over the experimental angular-momentum distribution for a proper comparison with the high-energy data.

It is very important to note that the neutron energy spectra should have negligible contamination from noncompound reactions to obtain the NLD using particle spectra. This is inferred by measuring the evaporated neutron spectra at backward angle where the contributions from direct and preequilibrium reactions are expected to be negligibly small. A previous study confirmed that the neutron energy spectra

measured at backward angles from α-induced reactions on different mass regions are mainly dominated by compound nuclear reactions [46–48]. In addition, the experimental fold distributions were generated during the off-line analysis by gating with the high-energy γ rays [49] to remove the nonfusion events, which generally appear for the lowest folds. It is observed that the fold distributions gated with high-energy γ rays and with neutrons are almost the same [49]. Therefore, the good matching between the simulated fold distribution (considering only CN angular momentum distribution) and experimental fold distribution [see Fig. 2(a)] also confirms the negligibly contribution from nonfusion events.

The error due to J distribution (± 4) is taken care of by using the extracted level density weighted over the experimental J distribution. The present technique for extracting the angular momentum gated level density could be well suited for lighter projectiles such as α particles at very low excitation energies, where the contribution from only one residue is significant or if the measurement could be carried out in coincidence with the evaporation residue. The importance of this measurement lies in the direct measurement of inverse level density parameter k at the experimental J and T as it is well known that k changes significantly with J and T [13–16]. The values of k, J, and T for different folds are shown in Fig. 6.
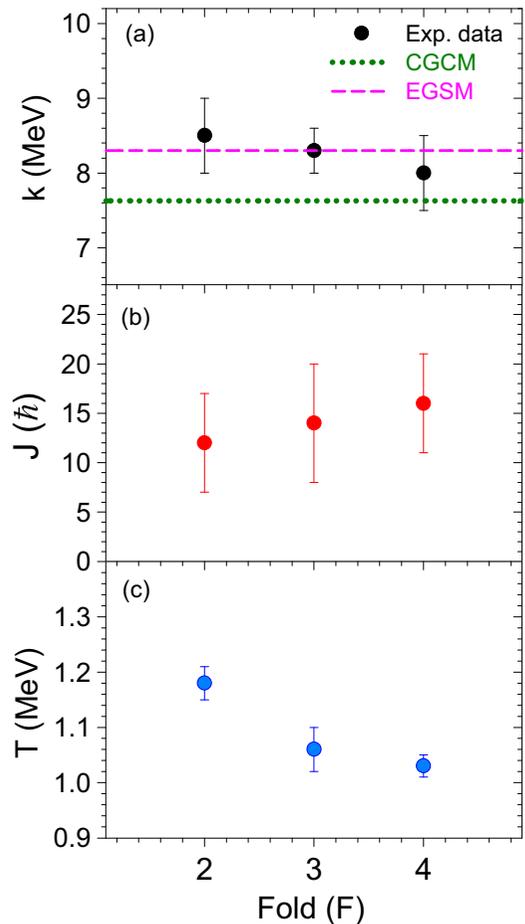

FIG. 6. The value of k, J and T for different folds. The dotted and dashed lines represent the k value according to CGCM [40] and EGSM [41], respectively, as discussed later in the text.
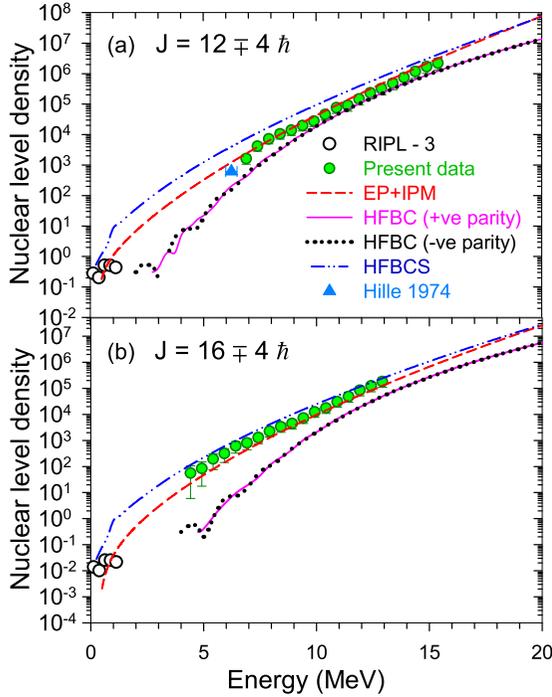
FIG. 7. Angular momentum gated NLD (filled cirlces) along with the results of different theoretical calculations. Open circles are taken from RIPL-3 [45] weighted over our J distribution and filled triangle is from Hille *et al.* [52].

It is evident from Fig. 7 that the EP+IPM NLDs agree well with the experimental data in both low- and higher-energy regions, whereas the NLDs obtained within the HFBCS can describe the experimental data at $J = 16\hbar$ only and those obtained within the HFBC underestimate the measured data. The reason is that the HFBCS violates the particle number and it does not also take into account thermal fluctuations, which are very important in finite systems as atomic nuclei [50]. As the result, to fit the experimental data, the NLDs obtained within the HFBCS and HFBC have to be renormalized to the known NLD data, namely the data extracted from the experimental analysis of the cumulative number of discrete levels at low E and the average neutron resonance spacing data at the neutron binding energy D_0 [43,44]. Unfortunately, the experimental value D_0 for the ^{96}Tc nucleus is not available at present. Therefore, the HFBCS NLD was normalized to the low-E data only and it certainly does not describe the high-E data as seen in Fig. 7. At the same time, by comparing the NLDs obtained from the HFBC in RIPL-3 [45] with those given in BRUSILB [51] within the same method but without renormalization, we found that the HFBC NLDs from these two libraries, which are shown in Fig. 7, are exactly the same. This indicates that, without renormalization, the HFBC completely fails to describe the NLD data. It should be mentioned here that no normalization is required within the EP+IPM as has been mentioned in detail in Ref. [29].

It is worthwhile noticing that the present experimental data are not normalized as there are no available data at finite angular momentum. Therefore, the NLD of ^{96}Tc at $E^* = 6$–6.5 MeV was estimated from Ref. [52] by using the experimentally

measured spin cutoff factor and the corresponding formula described there. The estimated value matches nicely with our level density [as shown in Fig. 7(a)]. It is observed that the present experimental data are about 12 times smaller in comparison to neighboring nuclei ^{95,96}Mo at $E^* = 6$ MeV ($J = 0\hbar$) due to the finite angular momentum selected in our experiment for ^{96}Tc. Our level density has also been compared with the results of microscopic EP+IPM calculation, which provides the absolute value of NLD and recently explained the level density in other mass regions without any normalization [29]. The good matching between the present experimental data and EP+IPM results provides the confidence on our measurement of NLD. Therefore, the EP+IPM results for the J-dependent NLDs shown in Fig. 7 together with those for the total NLDs reported in Ref. [29] clearly show that the EP+IPM method, which conserves exactly the particle number at both zero and finite temperature, is indeed a microscopic method able to provide a reliable description of both total and angular-momentum-dependent NLD data.

To obtain the NLD for the whole range of E^*, the composite Gilbert-Cameron model (CGCM) [40] has been used in the past. This model combines the constant temperature model at low E^* with Fermi gas model at higher E^* to get a realistic E^*-dependent NLD. The CGCM model gives $\tilde{a} = \alpha A + \beta A^{2/3}$, where A is the mass number, the parameters α and β are estimated as $\alpha = 0.0692559$ and $\beta = 0.282769$ [40], and thus the value of k comes as 7.63 MeV for ^{96}Tc. Another formalism of NLD exists, namely the enhanced generalized superfluid model (EGSM), which takes into account the E^* shifts, shell dependencies of NLD, and collective enhancement due to vibrational and rotational effects, within the framework of the nuclear superfluidity at low energy and Fermi gas at higher energy [41]. It gives the corresponding values of α and β as 0.093 ± 0.004 and 0.105 ± 0.014, respectively [53]. The E^* shift is estimated as $\delta_{\text{shift}} = 0.617 - 0.00164A$ MeV. In this case, k becomes 8.3 MeV for ^{96}Tc. The k values, based on EGSM and CGCM, have been plotted in Fig. 6(a), along with the experimental values. Our experimental data agree better with the EGSM values rather than with the CGCM ones. The higher value of experimental k indicates lower $\tilde{a}$ that in turn decreases the NLD. This could be explained in the light of the theory of fading out of collectivity in NLD, as the EGSM includes the collective enhancement of NLD [15,47–49]. This is corroborated by the agreement of experimental data with the results of EP+IPM microscopic calculations, which include the collective enhancement effect.

B. Spin cutoff factor

The ratio of experimental level densities at the same E^* but different J values allows us to extract the energy dependence of the spin cutoff factor (σ) as shown in Fig. 8, where the extracted σ as a function of excitation energy is compared with the theoretical approximation $\sigma_F^2 = 0.01389 \frac{A^{5/3}}{\tilde{a}} \sqrt{aU}$ [53] (shown as dotted line). The error bar in the experimental data is estimated from the errors of NLDs and J. Besides, the estimated σ by a frequently used theoretical prediction $\sigma^2 = 0.1461\sqrt{a(U-\delta)}A^{2/3}$ [6,54] with the pairing energy δ is also plotted in the same figure (dashed line). This prediction
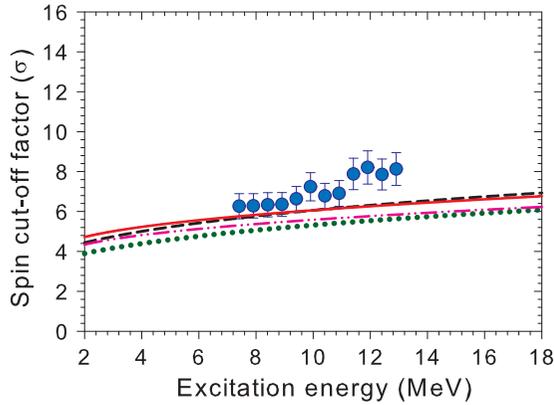
FIG. 8. Excitation energy-dependent spin cutoff factor (filled symbols) along with different theoretical calculations. The dotted lines are taken from Ref. [53], the dashed lines are taken from Ref. [54]. The continuous and double dot-dashed lines represent the $\sigma_\perp$ and $\sigma_\parallel$, respectively, used in the EP+IPM calculation.

is based on a statistical mechanical calculation, which averages the square of the spin projection on the z axis over the single-particle states near the Fermi level [6]. The experimental data are also compared with the results of the microscopic EP+IPM calculations by using the Eqs. (11) and (12) as shown by the continuous ($\sigma_\perp$) and double dot-dashed ($\sigma_\parallel$) lines, respectively, in Fig. 8. It is seen that the trend of the extracted σ is reproduced by the EP+IPM ($\sigma_\perp$) and the formulas given in Refs. [6,53,54].

C. Nuclear thermodynamical quantities

As the NLDs obtained within the EP+IPM agree well with the experimental data, they can be used to calculate the TQ in order to understand the behaviors of the latter as functions of T and J. The TQ of ^{96}Tc have been estimated using EP+IPM NLDs for $J = 12$ and 16 $\hbar$ as shown in Fig. 9. It can be seen from this figure that all the TQ show the correct trend as that observed in a nearby nucleus ^{96}Mo [11,12]. The free energy,

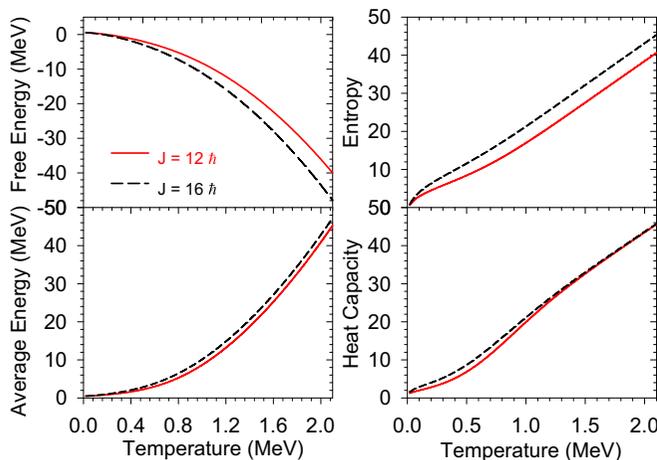FIG. 9. Angular momentum gated thermodynamic quantities as functions of temperature obtained using EP+IPM level densities.

entropy, and average energy behave smoothly as functions of temperature as expected. However, the nature of heat capacity in ^{96}Tc is different from ^{96}Mo nucleus, namely there is a pronounced bump in the heat capacity of ^{96}Mo at around $T \sim 0.7$–1 MeV, which is close to the critical temperature T_c where the pairing gap collapses [11,12]. As for the heat capacity of ^{96}Tc, a little bump is seen at around $T \sim 0.5$–1.0 MeV. This difference might come from the pairing property of odd-odd ^{96}Tc nucleus, which is weaker than that in even-even ^{96}Mo. It is also observed that the angular momentum does not have much effect on the nature of the TQ. Among the four TQ, the heat capacity is the most important quantity as it gives the useful information about the pairing phase transition. As can be seen from Fig. 9, the heat capacities for $J = 12$ and 16 $\hbar$ coincide at high temperature ($T > 1.5$ MeV). However, at low T, there is a noticeable change due to the angular momentum. Therefore, the angular momentum could have an important role in even-even systems or for those nuclei that show the pairing reentrance phenomena [55]. Thus, it would be very interesting to study the angular momentum effect on the pairing phase transition in even-even systems in the near future.

VI. SUMMARY AND CONCLUSIONS

Angular momentum gated NLDs in the energy range of $E^* = 5$–15 MeV have been extracted using the evaporated neutron energy spectra in the ^{4}He + ^{93}Nb reaction. The level density parameter and angular momentum were measured experimentally and used in the statistical model code to estimate the NLD. The use of a low-energy light-ion α beam allows us to extract the NLD at below and above the particle threshold energy. The extracted NLDs for $J = 12$ and 16 $\hbar$ were compared with the results of different microscopic calculations such as EP+IPM, HFBCS, and HFBC. It is observed that EP+IPM explains rather well the experimental data and thus it was used to extract the thermodynamic properties of ^{96}Tc nucleus. It is quite interesting to note that the free energy, entropy, and average energy show the correct trend as that observed in the nearby ^{96}Mo nucleus. However, the bump in the heat capacity of ^{96}Tc is not as pronounced as that seen in ^{96}Mo, in spite of being the same mass. This difference should not be a surprise since pairing in the even-even system as ^{96}Mo is always stronger than that in the odd-odd system as ^{96}Tc. In addition, although the angular momentum does not have much effect on the nature of thermodynamic quantities, it would be very interesting to study the angular momentum effect on pairing correlation in even-even systems. In addition, the E^*-dependent spin cutoff factor has also been extracted and is found to be in reasonable agreement with the well-known theoretical formulas.

[1] C. Bustamante, J. Liphardt, and F. Ritort, Phys. Today **58**, 43 (2005).

[2] E. Fermi, *Thermodynamics* (Courier Dover Publications, Mineola, 1956).

[3] H. A. Bethe, Phys. Rev. **50**, 332 (1936); Rev. Mod. Phys. **9**, 69 (1937).

[4] S. K. Ma, *Statistical Mechanics* (World Scientific, Singapore, 1985); M. Toda, R. Kubo, and N. Saito, *Statistical Physics I* (Springer Verlag, Berlin, 1992).

[5] J. Bardeen, L. N. Cooper, and J. R. Schrieffer, Phys. Rev. **108**, 1175 (1957).

[6] A. V. Ignatyuk, G. N. Smyrenkin, M. G. Itkis, S. I. Mulgin, and V. N. Okolovich, Sov. J. Part. Nuclei **16**, 307 (1985) [Fiz. Elem. Chastits At. Yadra **16**, 710 (1985)].

[7] A. Schiller, A. Bjerve, M. Guttormsen, M. Hjorth-Jensen, F. Ingebretsen, E. Melby, S. Messelt, J. Rekstad, S. Siem, and S. W. Odegard, Phys. Rev. C **63**, 021306(R) (2001).

[8] E. Melby *et al.*, Phys. Rev. Lett. **83**, 3150 (1999).

[9] M. Guttormsen, E. Melby, J. Rekstad, S. Siem, A. Schiller, T. Lonnroth, and A. Voinov, J. Phys. G **29**, 263 (2003).

[10] A. Schiller, L. Bergholt, M. Guttormsen, E. Melby, J. Rekstad, and S. Siem, Nucl. Instrum. Methods Phys. Res. A **447**, 498 (2000).

[11] R. Chankova, A. Schiller, U. Agvaanluvsan, E. Algin, L. A. Bernstein, M. Guttormsen, F. Ingebretsen, T. Lonnroth, S. Messelt, G. E. Mitchell, J. Rekstad, S. Siem, A. C. Larsen, A. Voinov, and S. Odegard, Phys. Rev. C **73**, 034311 (2006).

[12] K. Kaneko, M. Hasegawa, U. Agvaanluvsan, E. Algin, R. Chankova, M. Guttormsen, A. C. Larsen, G. E. Mitchell, J. Rekstad, A. Schiller, S. Siem, and A. Voinov, Phys. Rev. C **74**, 024325 (2006).

[13] S. Shlomo and J. B. Natowitz, Phys. Lett. B **252**, 187 (1990); Phys. Rev. C **44**, 2878 (1991).

[14] B. Dey *et al.*, Phys. Rev. C **91**, 044326 (2015).

[15] K. Banerjee *et al.*, Phys. Rev. C **85**, 064310 (2012).

[16] M. Gohil *et al.*, Phys. Rev. C **91**, 014609 (2015).

[17] A. V. Voinov, S. M. Grimes, A. C. Larsen, C. R. Brune, M. Guttormsen, T. Massey, A. Schiller, S. Siem, and N. U. H. Syed, Phys. Rev. C **77**, 034613 (2008).

[18] A. V. Voinov, S. M. Grimes, U. Agvaanluvsan, E. Algin, T. Belgya, C. R. Brune, M. Guttormsen, M. J. Hornish, T. Massey, G. E. Mitchell, J. Rekstad, A. Schiller, and S. Siem, Phys. Rev. C **74**, 014314 (2006).

[19] K. Banerjee *et al.*, Nucl. Instrum. Methods Phys. Res. A **608**, 440 (2009).

[20] D. Pandit *et al.*, Nucl. Instrum. Methods Phys. Res. A **624**, 148 (2010).

[21] S. Agostinelli *et al.*, Nucl. Instrum. Methods Phys. Res. A **506**, 250 (2003).

[22] F. Puhlhofer, Nucl. Phys. A **280**, 267 (1976).

[23] A. V. Ignatyuk, G. N. Smirenkin, and A. S. Tishin, Sov. J. Nucl. Phys. **21**, 255 (1975).

[24] C. M. Perey and F. G. Perey, At. Data Nucl. Data Tables **17**, 1 (1976).

[25] F. G. Perey, Phys. Rev. **131**, 745 (1963).

[26] L. Mcfadden and G. R. Satchler, Nucl. Phys. A **84**, 177 (1966).

[27] D. R. Chakrabarty, V. M. Datar, S. Kumar, E. T. Mirgule, H. H. Oza, and U. K. Pal, Phys. Rev. C **51**, 2942 (1995).

[28] A. P. D. Ramirez, A. V. Voinov, S. M. Grimes, A. Schiller, C. R. Brune, T. N. Massey, and A. Salas-Bacci, Phys. Rev. C **88**, 064324 (2013).

[29] N. Quang Hung, N. Dinh Dang, and L. T. Quynh Huong, Phys. Rev. Lett. **118**, 022502 (2017).

[30] A. Volya, B. A. Brown, and V. Zelevinsky, Phys. Lett. B **509**, 37 (2001).

[31] N. Quang Hung and N. Dinh Dang, Phys. Rev. C **79**, 054328 (2009).

[32] Y. Alhassid, G. F. Bertsch, and L. Fang, Phys. Rev. C **68**, 044322 (2003).

[33] T. Ericson, Adv. Phys. **9**, 425 (1960).

[34] G. Maino, E. Menapace, and A. Ventura, Nouvo Cimeto A **57**, 427 (1980); G. Maino, M. Vaccari, and A. Ventura, Comput. Phys. Commun. **29**, 375 (1983).

[35] L. G. Moretto, Nucl. Phys. A **182**, 641 (1972); **185**, 145 (1972).

[36] W. Dilg, W. Schantl, H. Vonach, and M. Uhl, Nucl. Phys. A **217**, 269 (1973).

[37] A. R. Junghans *et al.*, Nucl. Phys. A **629**, 635 (1998); M. N. Nasrabadi and M. Sepiani, Acta Phys. Pol. B **45**, 1865 (2014).

[38] A. Bohr and B. R. Mottelson, *Nuclear Structure* (Benjamin, New York, 1969), Vol. 1.

[39] S. Cwiok *et al.*, Comput. Phys. Commun. **46**, 379 (1987).

[40] A. Gilbert and A. G. W. Cameron, Can. J. Phys. **43**, 1446 (1965).

[41] A. D'Arrigo, G. Giardina, M. Herman, A. V. Ignatyuk, and A. Taccone, J. Phys. G: Nucl. Part. Phys. **20**, 365 (1994).

[42] N. Quang Hung, N. Dinh Dang, and L. T. Quynh Huong, Phys. Rev. C **94**, 024341 (2016).

[43] P. Demetriou and S. Goriely, Nucl. Phys. A **695**, 95 (2001).

[44] S. Hilaire and S. Goriely, Nucl. Phys. A **779**, 63 (2006); S. Goriely, S. Hilaire, and A. J. Koning, Phys. Rev. C **78**, 064307 (2008).

[45] https://www-nds.iaea.org/RIPL-3/.

[46] K. Banerjee *et al.*, Phys. Lett. B **772**, 105 (2017).

[47] P. Roy *et al.*, Phys. Rev. C **86**, 044622 (2012).

[48] P. Roy *et al.*, Phys. Rev. C **94**, 064607 (2016).

[49] B. Dey *et al.*, Phys. Lett. B **731**, 92 (2014).

[50] L. G. Moretto, Phys. Lett. B **40**, 1 (1972); A. L. Goodman, Phys. Rev. C **29**, 1887 (1984); N. Dinh Dang and V. Zelevinsky, *ibid.* **64**, 064319 (2001); N. Dinh Dang and A. Arima, *ibid.* **67**, 014304 (2003); **68**, 014318 (2003); N. Dinh Dang, Nucl. Phys. A **784**, 147 (2007).

[51] http://www.astro.ulb.ac.be/bruslib/index.html.

[52] P. Hille, P. Sperr, M. Hille, K. Rudolph, W. Assmann, and D. Evers, Nucl. Phys. A **232**, 157 (1974).

[53] R. Capote *et al.*, Nucl. Data Sheets **110**, 3107 (2009).

[54] T. von Egidy and D. Bucurescu, Phys. Rev. C **80**, 054310 (2009).

[55] N. Quang Hung, N. Dinh Dang, B. K. Agrawal, V. M. Datar, A. Mitra, and D. R. Chakrabarty, Acta Phys. Pol. B Proceedings Supplement **8**, 551 (2015).